Received: 13 March 2023 | Revised: 22 September 2023 | Accepted: 24 September 2023

DOI: 10.1002/hyp.15008

RESEARCH ARTICLE

WILEY

Combining Landsat TIR-imagery data and ERA5 reanalysis information with different calibration strategies to improve simulations of streamflow and river temperature in the Canadian Subarctic

Eisinhower Rincón [1] | André St-hilaire [1,2] | Normand E. Bergeron [1] | Stephen J. Dugdale [3]

[1]Centre Eau Terre Environnement, Institut National de la Recherche Scientifique (INRS), Québec, Québec, Canada

[2]Canadian Rivers Institute, Fredericton, New Brunswick, Canada

[3]School of Geography, University of Nottingham, Nottingham, UK

Correspondence
Eisinhower Rincón, Centre Eau Terre Environnement, Institut National de la Recherche Scientifique (INRS), 490 de la Couronne Street, Québec City, Qc G1K 9A9, Canada.
Email: eisinhower.rincon@inrs.ca

Funding information
Government of Canada

Abstract

Arctic and Subarctic environments are among the most vulnerable regions to climate change. Increases in liquid precipitation and changes in snowmelt onset are cited as the main drivers of change in streamflow and water temperature patterns in some of the largest rivers of the Canadian Arctic. However, in spite of this evidence, there is still a lack of research on water temperature, particularly in the eastern Canadian Arctic. In this paper, we use the CEQUEAU hydrological-water temperature model to derive consistent long-term daily flow and stream temperature time series in Aux Mélèzes River, a non-regulated basin (41 297 km^2) in the eastern Canadian subarctic. The model was forced using reanalysis data from the fifth-generation ECMWF atmospheric reanalyses (ERA5) from 1979 to 2020. We used water temperature derived from thermal infrared (TIR) images as reference data to calibrate CEQUEAU's water temperature model, with calibration performed using single-site, multi-site, and upscaling factors approaches. Our results indicate that the CEQUEAU model can simulate streamflow patterns in the river and shows excellent spatiotemporal performance with Kling-Gupta Efficiency (KGE) metric >0.8. Using the best-performing flow simulation as one of the inputs allowed us to produce synthetic daily water temperature time series throughout the basin, with the multi-site calibration approach being the most accurate with root mean square errors (RMSE) <2.0°C. The validation of the water temperature simulations with a three-year in situ data logger dataset yielded an RMSE = 1.38°C for the summer temperatures, highlighting the robustness of the calibrated parameters and the chosen calibration strategy. This research demonstrates the reliability of TIR imagery and ERA5 as sources of model calibration data in data-sparse environments and underlines the CEQUEAU model as an assessment

tool, opening the door to its use to assess climate change impact on the arctic regions of Canada.

KEYWORDS
arctic rivers, CEQUEAU, PUB, reanalysis, thermal infrared, water temperature

1 | INTRODUCTION

Water temperature is one of the most critical variables for freshwater ecosystems because it strongly influences biological, physical, and chemical processes within rivers (Caissie, 2006; Hannah & Garner, 2015; Webb et al., 2008). Key biophysical properties, such as dissolved oxygen (Ficklin et al., 2013) and the growth of living organisms (Hette-Tronquart et al., 2013; Isaak & Rieman, 2013) are largely controlled by river temperature (Caissie, 2006).

In the Northern Hemisphere, future climate projections indicate that Arctic and Subarctic regions will undergo changes in the variability and intensity of climate and weather conditions that will likely be much greater than the rest of the world (Larsen et al., 2014). In northern Canada, global warming has been identified as the main driver responsible for the positive annual and seasonal trends in air temperature during the last decades (DeBeer et al., 2016). Specifically, the current observed warming in the northeastern region of Canada (and more broadly, the entire Arctic) is directly attributable to anthropogenic forcing (Ding et al., 2014). Changes in the snowmelt onset (Foster et al., 2008), spatial precipitation patterns (Vaughan et al., 2013) and permafrost thaw (Hinzman et al., 2005) related to this warming will inevitably impact freshwater systems with substantial socio-ecological implications (Bolduc & Lamoureux, 2018; Dugdale et al., 2018; Hill et al., 2014; van Vliet et al., 2013). Global hydrological model simulations have shown that Arctic basins will experience notably higher flows due to significant increases in precipitation and snowmelt (van Vliet et al., 2013). In particular, northwest Canadian rivers exhibited a significant upward trend in winter baseflow and increases of mean annual flow, perhaps due to permafrost thawing (St. Jacques & Sauchyn, 2009). Although there are fewer studies in the eastern portion of the country, similar changes are expected. Furthermore, the development of large hydroelectric projects in northeastern Canada has significantly decreased the discharge of large watersheds such as the Caniapiscau River, because of the diversion of its flow into the La Grande Rivière system (Déry et al., 2016). These changes in flow regimes have been identified as an important driver of riverine thermal dynamics in arctic rivers located in northwest Canada (e.g., Yang et al., 2021) as well as in some notable rivers in the southeastern regions (e.g., Charron et al., 2021). However, in spite of the demonstrated importance of thermal regimes for arctic rivers, there is still a lack of information and studies about Arctic and Subarctic rivers in eastern Canada, even knowing that changes in river water temperature can be harmful to numerous freshwater fish species, particularly salmonids (Klemetsen et al., 2003; Reist, Wrona, Prowse, Power, Dempson, Beamish, et al., 2006; Reist, Wrona, Prowse, Power, Dempson, King, et al., 2006; Svenning et al., 2016).

Arctic regions are challenging to study, given the complexities related to data collection (Yang et al., 2014; Yang & Peterson, 2017). Although ground-based observations of water temperature and streamflow have been gathered since the 20th century (e.g., Lammers et al., 2001), high spatial and temporal resolution measures are often required to fill gaps and elucidate, quantitatively, the impacts of climate change on Arctic rivers (Hori, 2021). Applications of satellite-derived products hold potential for filling this gap in northern regions since they have been applied to retrieve hydrological and thermal information from low- and mid-latitude rivers (Martí-Cardona et al., 2019; Tavares et al., 2019, 2020). In tandem with the potential of satellite data, reanalysis datasets have been extensively used as reference meteorological data to describe phases of the hydrological cycle in data-sparse basins (e.g., Essou et al., 2016; Jiang et al., 2021; Krogh et al., 2015; Tarek et al., 2020). Overall, reanalyses have been confirmed as a reliable source of information, especially if, for example, no or few land surface stations are available in the study area. Tarek et al. (2020) found that ERA5 reanalysis performs very well in North America, and simulations with a hydrological model forced with these data sets matched the observed values. Similarly, Krogh et al. (2015) found that ERA-Interim is a good source of meteorological information to calibrate hydrological models in two basins in southern Chile, where monitoring is very challenging. More recently, Gatien et al. (2022) used ERA5 and ERA5-Land to evaluate the performance of HEC-RAS to simulate the hydraulic and water temperature conditions on a large reservoir in a date-sparse region in western Canada, finding that the model was able to produce high-quality hydraulic and water temperature simulations when it is forced with this reanalysis products.

This work is framed in the context of predictions in ungauged basins (PUB, Sivapalan et al., 2003; Hrachowitz et al., 2013). Here we focus on deriving modelled water temperature time series as an alternative to long-term in-situ observations in arctic regions. We take the Aux Mélèzes River, Nunavik, Canada as a case study and use CEQUEAU, a semi-distributed model that can simulate both flow and water temperature as our selected simulation tool. Our specific objectives are (1) to derive high-quality water temperature time series from spaceborne thermal infrared imagery, (2) to use these data to calibrate the CEQUEAU model, comparing a range of calibration strategies: single-site calibration, multi-ensemble parameter averaging (upscaling factors), and multi-site calibration; and (3) to derive consistent spatially distributed long-term water temperature time series in a

TABLE 1 CEQUEAU variables obtained from ERA5 reanalyses.

Variable	Description	Units
pTot	Total daily precipitation	mm
tMax	Maximum daily air temperature	°C
tMin	Minimum daily temperature	°C
rad	Incoming net solar radiation	MJ m^{-2}
vp	Vapour pressure	mmHg
w	Wind speed	Km h^{-1}
cc	Cloud cover	%

Note: The units are the input unit for the CEQUEAU model.

data-sparse region. This represents the first attempt to derive long-term water temperature time series in Aux Mélèzes River and the first exercise of using spaceborne information to calibrate the CEQUEAU water temperature model.

2 | METHODS

2.1 | The CEQUEAU model

CEQUEAU is a process-based, coupled, semi-distributed hydrological/water temperature model (Morin & Paquet, 2007; St Hilaire et al., 2015; St-Hilaire et al., 2000). The model simulates daily river flow and water temperature by subdividing the watershed into a series of whole squares (hereafter CE for the French abbreviation for *Carreaux Entiers*, following the model's documentation). For each CE, the altitude, the percentage of the forest, and the percent area covered by lakes and wetlands are computed. Each CE is further subdivided into a maximum of four polygons called partial squares (hereafter CP for the French abbreviation of *Carreaux Partiels*) based on the sub-basins division of the watershed. The hydrological model comprises two functions (shown in Figure S1 in the Supplementary material) to calculate the water budget throughout the basin: the production function, which calculates water availability for river routing in each CP at each time step and the transfer function, which manages the upstream-downstream water routing at each time step (Morin & Paquet, 2007). The main equations describing the CEQUEAU model production functions and the routing functions are presented in S1 and S3, respectively. Also, the hydrological model parameters can be found in Table S1 of the supplementary material.

The CEQUEAU water temperature uses the results from the hydrological model to calculate the water temperature. For each CE at a time-step t, the change in water temperature (ΔT_{w_t} in°C) is given by the Equation (1):

$$\Delta T_{w_t} = \frac{\Delta Q_t}{V_t \cdot \Theta}, \tag{1}$$

where ΔQ_t is the total change in enthalpy (MJ), V is the volume of water (m^3) and $\Theta = 4.187$ MJ $m^{-3}{}^{\circ}C^{-1}$ which is the heat capacity of the water. The term ΔQ_t in Equation (1) is the result of the surface energy budget, which is computed at any time-step t as follows:

$$Q_t = Q_{sw_t} + Q_{lw_t} + Q_{e_t} + Q_{s_t} + Q_{a_t}, \tag{2}$$

where Q_{sw_t} is the flux of incoming solar short-wave radiation, Q_{lw_t} is the longwave radiative flux, Q_e is the latent heat transfer, Q_{s_t} is the sensible heat transfer and Q_{a_t} is the advective heat transfer from the upstream grid squares and groundwater and subsurface flow. The terms of Equation (2) are depicted in Equations (S5)–(S7) in the supplementary material. The meteorological inputs for the CEQUEAU model are listed in Table 1.

The hydrological module has 31 parameters, of which 25 are fitted, and the remaining are constants and dependent on the physiographic characteristics of the watershed (see Table S1 in the supplementary material), while the water temperature module requires 10 parameters to be fitted. The description of the hydrological parameters is presented in Table S1 in the supplementary material, and the water temperature module parameters are presented in Table 2.

2.2 | Study region

Aux Mélèzes River is located in the eastern Canadian Subarctic in Nunavik, Quebec, Canada (Figure 1). It flows directly into the Koksoak River, which empties into Ungava Bay. The Ungava is home to several indigenous communities whose traditional subsistence activities revolve around hunting, gathering, and fishing (Parlee & Furgal, 2012). This region has also been important for fisheries during the last two centuries (Power, 1976), an activity that is strikingly threatened by climate change (Poesch et al., 2016).

The Aux Mélèzes River is a large unregulated basin that drains an area of approximately 41 297 km^2. According to the North American Land Change Monitoring System (NALCMS), land use within the catchment comprises a significant proportion (56.86%) covered by shrublands and grasslands. Another substantial portion of 24.18% is covered by forest, and surface water bodies make up the additional 8.98%. The NALCMS dataset was used to parameterize CEQUEAU with Aux Mélèzes River basin physiography and is freely available through the following link: http://www.cec.org/north-american-environmental-atlas/land-cover-2010-landsat-30m/. For this river, we used a model grid size of 8 × 8 km to define the CEs, from which CPs are subsequently delineated according to water divide and drainage. This grid resolution was chosen as a trade-off to maximize the resolution and minimize the model run-time (Dugdale et al., 2017) for a total of 796 and 915 CEs and CPs, respectively.

2.3 | Meteorological and hydrometric data

Aux Mélèzes River has two gauge stations, one at the outlet point located in the CP-1 and a second one in an upstream sub-basin

TABLE 2 Hydrological model parameters.

No	Parameter	Description	Units	Lower bound	Upper bound
1	COPROM	Fitting coefficient to determine the minimum depth of the river reach	–	1.00	2.00
2	COLARG	Fitting coefficient to adjust the river width	–	1.00	2.00
3	CRAYSO	Fitting coefficient for incoming solar radiation	–	1.00	2.00
4	CRAYIN	Fitting coefficient for shortwave radiation flux	–	1.00	3.00
5	CEVAPO	Fitting coefficient for latent heat flux	–	0.50	2.00
6	CCONVE	Fitting coefficient for sensible heat flux	–	1.00	2.00
7	CRIGEL	Threshold for snow stock controlling water temperature	mm	50.00	250.00
8	TNAP	Groundwater temperature	°C	4.00	8.00
9	BASSOL	Minimum precipitation to define days with low solar radiation	mm	5.00	10.00
10	CORSOL	Correction factor for BASSOL	–	0.00	1.00

located in the CP-213 (see Figure 1 for the location of the mentioned CPs). A description of the data for each station is given in Table 3.

To our knowledge, no meteorological stations exist, but one water temperature station located at the outlet point of the river (CP-1) administrated by the Québec Ministère des Forêts, de la Faune et des Parcs (MFFP) was used for validation purposes. The discharge data are freely available through the website of the Québec Ministère de l'Environnement et de la Lutte contre les changements climatiques (https://www.cehq.gouv.qc.ca/hydrometrie/historique_donnees/default.asp). Given the data scarcity, we used ERA5 reanalysis information available on the European Center for Medium-Range Weather Forecasts (ECMWF) website (https://www.ecmwf.int/en/forecasts/datasets/reanalysis-datasets/era5) with a native grid resolution of 0.25°×°0.25° covering the entire globe. ERA5 data are obtained by combining advanced modelling and data assimilation to generate the state of the atmosphere at a sub-daily time scale. This reanalysis has proved to be a reliable data source for hydrological simulations (Tarek et al., 2020) as well as for water temperature simulations (Gatien et al., 2022; Khorsandi et al., 2022).

2.4 | Hydrological model calibration

The typical strategy for calibrating the CEQUEAU model consists of first calibrating the hydrological module, then calibrating the water temperature module using the simulated flows as inputs (Charron et al., 2021; Khorsandi et al., 2022; Kwak et al., 2016, 2017; St-Hilaire et al., 2000). To fit the model parameters, we used the Covariance Matrix Adaptation Evolution Strategy (CMA-ES) (Hansen & Ostermeier, 2001), which is a stochastic non-linear optimization algorithm that is efficient in finding the optimum parameter value for the CEQUEAU model (Arsenault et al., 2014; Khorsandi et al., 2022).

We used the entire available period with concomitant meteorological and hydrometric data (1979–2020) to calibrate the hydrological model without splitting it into calibration and validation periods, as it provides the most robust results according to Shen et al. (2022). This calibration was made using the gauging station located at CP-1. The calibrated parameters were then validated using the gauging station at CP-213. We evaluated the performance of the model using the Nash–Sutcliffe (NSE, Nash & Sutcliffe, 1970) and Kling–Gupta (KGE, Gupta et al., 2009) efficiency coefficients, which are shown in Equations (3) and (4), respectively.

$$NSE = 1 - \frac{\sum_{i=1}^{n} (\hat{y}_t - y_t)^2}{\sum_{i=1}^{n} (\hat{y}_t - \overline{y}_t)^2}, \tag{3}$$

$$KGE = 1 - \sqrt{(r-1)^2 + \left(\frac{\hat{\sigma}}{\sigma} - 1\right)^2 + \left(\frac{\hat{\mu}}{\mu} - 1\right)^2}, \tag{4}$$

where $\hat{y}$ is the simulated value in the time step t, y is the observed value in the time step t, $\overline{y}$ is the average value of the observed time series, r is the linear correlation, $\hat{\sigma}$ and σ are the simulated and observed standard deviations, respectively, $\hat{\mu}$ and μ are the simulated and observed mean values, respectively. μ and $\overline{y}$ are equivalent values.

2.5 | Water temperature simulation

The water temperatures used to calibrate CEQUEAU's temperature module were extracted from thermal infrared (TIR) images acquired by Landsat missions 5, 7, and 8. Conversion from TIR radiance to water temperature was performed using the Statistical Mono-Window (SMW) Algorithm. The SMW algorithm was developed by The Satellite Application Facility on Climate Monitoring (CM-SAF, Duguay-Tetzlaff et al., 2015, 2017) This algorithm uses an empirical approach that relates the brightness temperature at the top of the atmosphere (TOA) of a single atmospheric window channel to land surface temperature (LST) via simple linear regression. The SMW algorithm linearizes the radiative transfer equation while maintaining the explicit

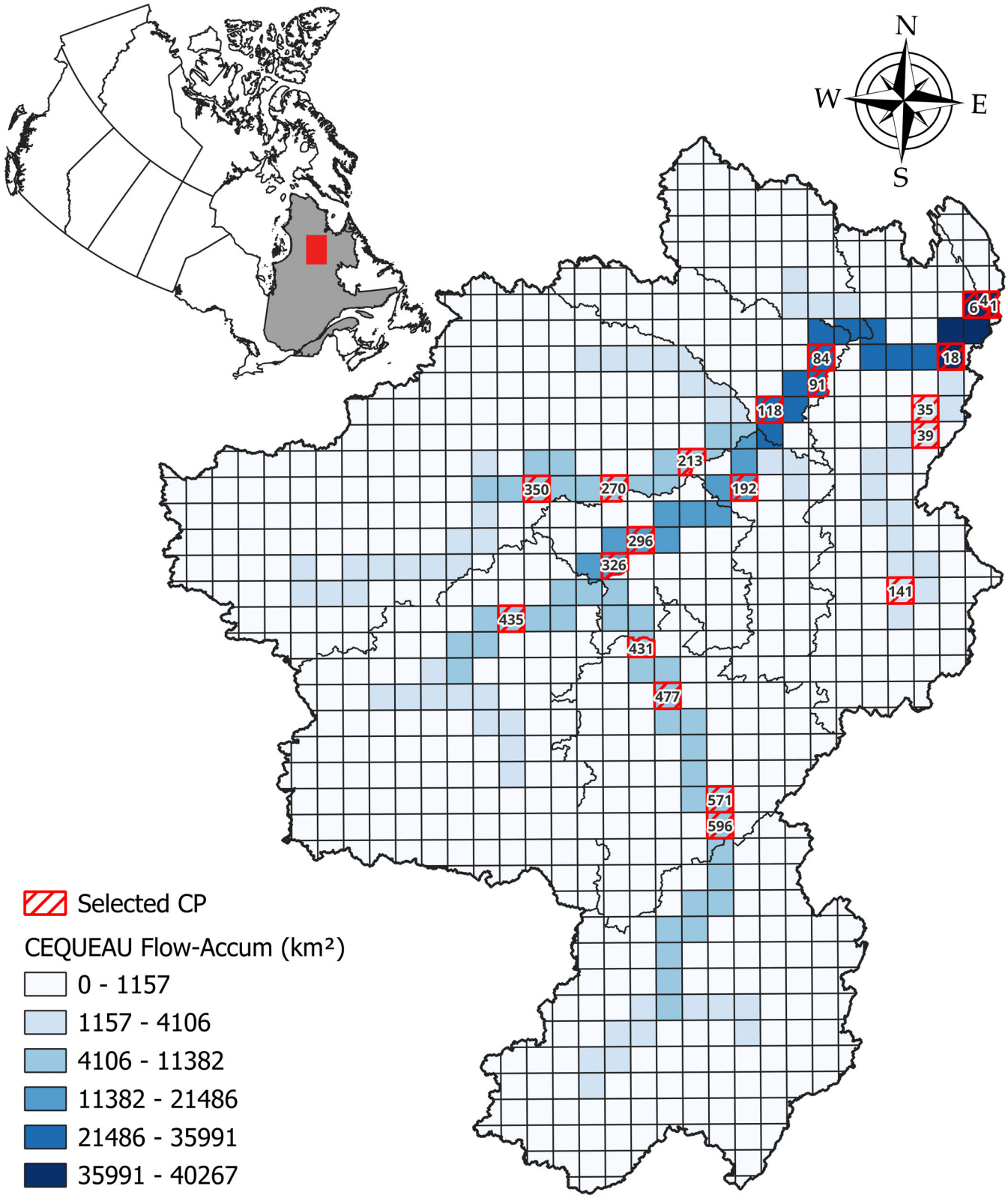

FIGURE 1 The Aux Mélèzes River showing the CEQUEAU model grid structure, with CPs used for calibration of the water temperature module highlighted.

Station ID	CP location	Date range	Frequency	Missing data
103 603	CP-1	1979/01–1993/07	Daily	13%
103 605	CP-213	1962/08–2019/09	Daily	24%

TABLE 3 Gauging station information.

dependency on surface temperature (Duguay-Tetzlaff et al., 2015) as shown in Equation (5):

$$LST = A_i + \frac{T_b}{\varepsilon} + B_i \frac{1}{\varepsilon} + C_i, \quad (5)$$

where T_b is the TOA brightness temperature (K) in the TIR channel and ε is the spectral surface emissivity. To avoid bias due to the estimation of the surface emissivity and knowing that the targeted pixels are picturing water, the value of the emissivity was set to 0.99 (Daigle et al., 2022).

The coefficients A_i, B_i and C_i are determined via simple linear regression throughout a calibration process of simulation of the radiative transfer equation performed for 10 classes ($i = 1, 2 \ldots 10$) of total column water vapour (TCWV, Ermida et al., 2020). Values obtained for Ermida et al. (2020) for the different Landsat missions were used in the present study. For further details on the contention of these coefficients, refer to Ermida et al. (2020) and references therein.

2.6 | Calibration strategies

During recent decades, the integration of airborne and spaceborne sensors along with hydrological and water temperature models has become very popular among hydrologists. For example, satellite-based instruments have been successfully applied to calibrate a water temperature model (Tavares et al., 2020) in the United States and evapotranspiration fluxes in western Central Africa (Odusanya et al., 2018). (Morales-Marín et al., 2019) used Landsat satellites as reference information to simulate the water temperature in the Canadian Prairies. However, the application of such techniques has never been tested in data-sparse Arctic river environments prone to strong seasonal variability, nor using the CEQUEAU model.

To correctly estimate river temperature using TIR images, a minimum of three pixels covering the river's width is required (as recommended in the literature; e.g., Cherkauer et al., 2005; Handcock et al., 2006) to reduce the radiative bank effect on centerline temperatures, given that mixed pixel effects are usually found along river banks (Cherkauer et al., 2005; Martí-Cardona et al., 2019). This normally reduces the applicability of the Landsat TIR images (60–120 m resolution) to rivers of 180–360 m in width. However, the recent algorithm developed by Martí-Cardona et al. (2019) showed that this limitation can be overcome by filtering out mixed pixels based on the earth-exiting thermal radiance of the Landsat scene. Using this approach, it is now possible to use Landsat to measure the temperature of rivers with widths as narrow as 120 m (Martí-Cardona et al., 2019). Taking the derived water temperature with the SMW algorithm described in Section 2.5, we applied the algorithm proposed by Martí-Cardona et al. (2019) to filter out mixed water-land pixels within each scene to avoid the effect of reflected radiance near the bank to retrieve reliable water temperatures distributed throughout the basin.

Given our CEQUEAU model's spatial discretization (8 × 8 km), it is in theory possible to map for every single CP a water temperature value from the Landsat images. However, as mapping water temperature for each CP in the CEQUEAU structure would be unnecessarily expensive in computational terms, we choose to calculate Root Mean Square Error (RMSE) at 21 distributed sites highlighted in red in Figure 1.

2.6.1 | Single site calibration strategy

We tested several different strategies for calibrating CEQUEAU's water temperature model. The first calibration approach we implemented is the single-site strategy (SSS). This is the traditional approach used by researchers and modellers, and consists of calibrating the CEQUEAU temperature module by using each of the individual selected CP sites separately. We used the Root Mean Square Error (RMSE) as the objective function, as the strong seasonality of river temperature inhibits the use of other metrics (e.g., NSE and KGE) commonly used for assessing the performance of discharge (rather than temperature) simulations (Ouellet-Proulx et al., 2019). The RMSE for a given CP is estimated using the Equation (6).

$$RMSE = \sqrt{\frac{1}{n}\sum_{i=1}^{n} (\hat{y}_t - y_t)^2}, \quad (6)$$

where $\hat{y}_t$ and y_t are the simulated and observed values at each time step, respectively.

2.6.2 | Upscaling factors calibration strategy

The second calibration strategy is the Upscaling Factors Strategy (UFS). The UFS takes the different sets of locally calibrated parameters using the SSS and combines them all using the upscaling factors proposed by Samaniego et al. (2010) to obtain one final set of parameters. This approach suggests that we can derive global parameters from a set of local parameters obtained from different SSS. This approach has recently been applied for CEQUEAU by Khorsandi et al. (2022). In this study, we used the Arithmetic, Harmonic, and Geometric means as upscaling factors. For further details, we suggest reading Samaniego et al. (2010) and the references therein.

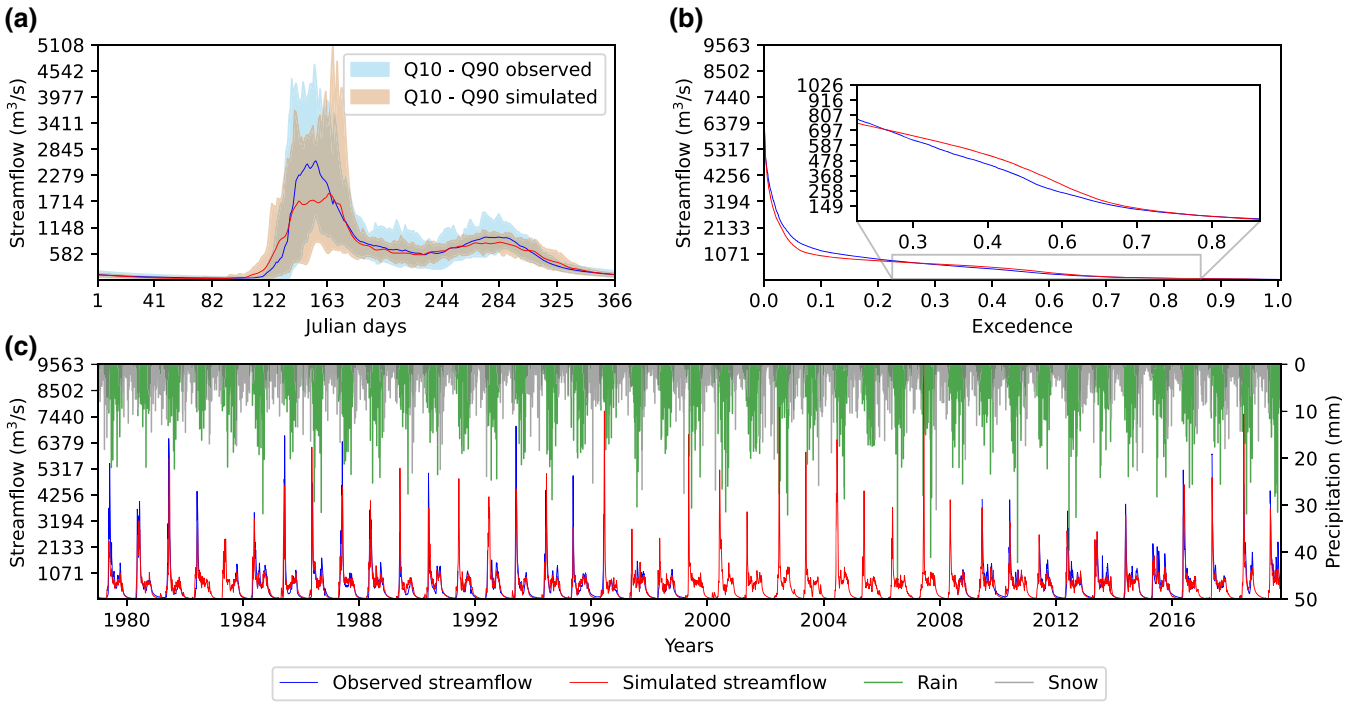

FIGURE 2 Comparison between the observed (blue line in station ID 103605) and simulated (red line in CP-1) streamflow in the Aux Mélèzes from 1979 to 2020. (a) represents the long-term multi-annual averaged observed and simulated hydrographs. The envelopes show the 10th and 90th percentile for simulated and observed flow, (b) represents the observed and simulated daily duration curves and (c) shows the daily observed and simulated streamflow time series. The precipitation shown in the (c) panel is partitioned between snow (grey lines) and rain (green lines) and represents the averaged total precipitation in CE-1. (KGE = 0.86, NSE = 0.79, RMSE = 348.66 m^3/s and BIAS = −45.64 m^3/s).

2.6.3 | Multi-site calibration strategy

The third approach used in this study is the multi-site strategy (MSS). This method consists of taking into account all the CPs during the calibration period. Two ways of multi-site calibration were used: (1) pooling all CPs together into a single, larger calibration database of water temperatures, which subsequently serves as the reference data to be evaluated with Equation (6), and (2), using a weight factor to give importance to the CP based on the length of the observed time series and the accumulated area downstream. This weighted objective function is shown in Equation (7)

$$RMSE_w = \frac{\sum_{i=1}^{n} RMSE_i \cdot M_i}{\sum_{i=1}^{n} M_i}, \quad (7)$$

where $i = 1,2,3...n$ as the ordinal number for each CP within the CEQUEAU model structure, $RMSE_i$ is the calculated RMSE using 6 for the ith CP and M_i refers to the weighting factor that can be either the accumulated area or the length of the available water temperature time series. These weights can be found in Table S2 of the Supplementary material. The previous procedure effectively constitutes a multi-site objective function through which we can calibrate our model.

2.7 | Water temperature validation

Following the establishment of the optimal calibration parameter set, the performance of CEQUEAU's water temperature simulations were validated by comparing the simulated temperatures against water temperature observations (summer 2015–autumn 2019) from the MFFP's temperature monitoring station (see Section 2.3).

3 | RESULTS

3.1 | Hydrological model calibration

Results of the hydrological calibration indicate that CEQUEAU represents flows in the Aux Mélèzes River with a good degree of accuracy (KGE = 0.86 and NSE = 0.79). The comparison between the simulated and observed flows from 1979 to 2020 at the most downstream point of the basin is presented in Figure 2. The model correctly simulated the recession curves during the end of spring (Apr–Jun) and the beginning of winter (Oct–Nov) as shown by the interannual hydrograph (Figure 2a), although there is a misrepresentation during the beginning of snowmelt. The model performs well in representing the seasonality of the two high peak flows during the snowmelt onset and the autumn rainfall (Figure 2c). However, the highest peaks are underestimated, especially during the period 1980–1999, where the

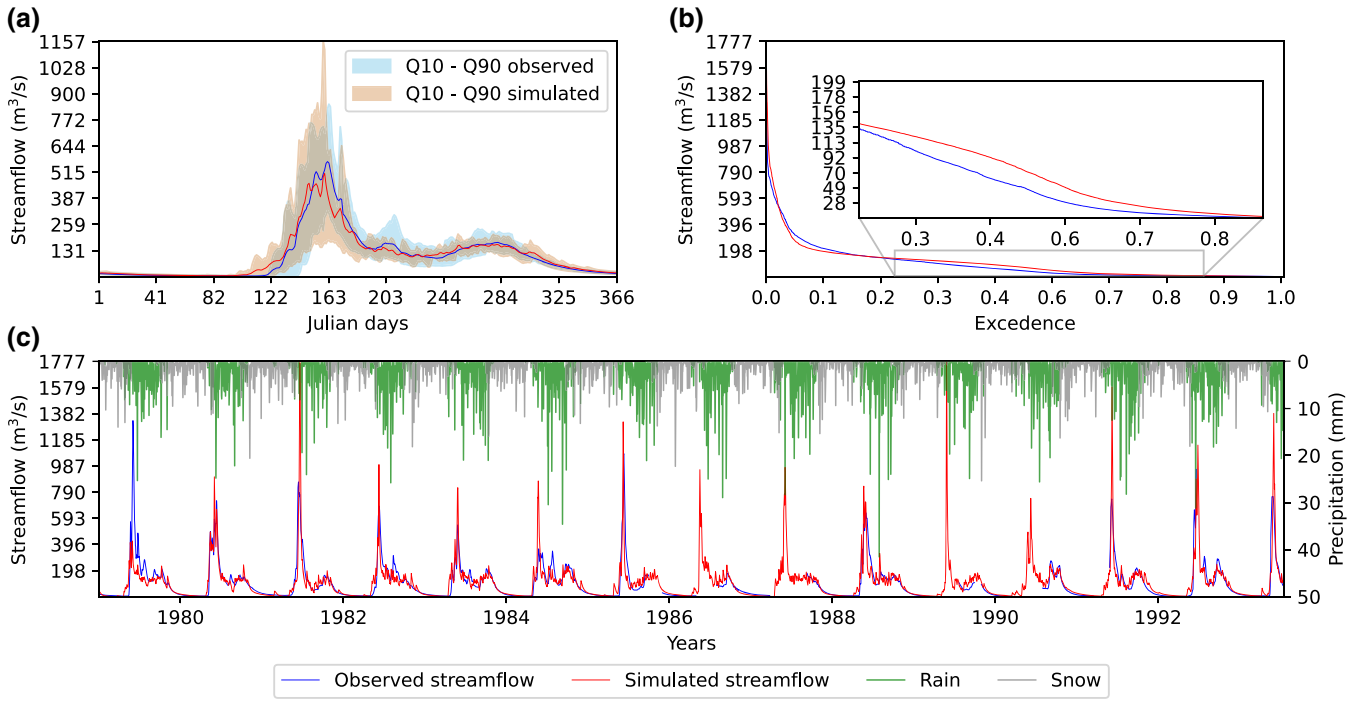

FIGURE 3 Same as Figure 2 but for the station ID 103603, CP-213 and CE-184 from 1979 to 1993. (KGE = 0.79, NSE = 0.65, RMSE = 80.75 m^3/s and BIAS = −1.5 m^3/s).

higher variability was exhibited. Given our interest in mainly the summer flows and water temperature, our calibrated parameters allowed us to correctly represent the flow values throughout the considered time period. The flow duration curve (Figure 2b) suggests that in spite of the model not correctly catching the distribution of the maximum values, it accurately represents the mean values during the whole period. This agreement was confirmed by computing the relative RMSE for the whole simulation period (RRMSE = 14.54%).

Figure 3 shows the results of our hydrological model validation, conducted by comparing simulations at CP-213 to streamflow observations at the corresponding gauging station (ID 103603) from 1979 to 1993. The obtained performance metrics (KGE = 0.79, NSE = 0.65, and RMSE = 80.75 m^3/s) show that the CEQUEAU model correctly represents the streamflow in this station even when the reference for calibrating the model was the outlet point. This obtained value indicates that any biases in our subsequent water temperature simulations relating to flow volume will likely be minimal.

3.2 | Water temperature model calibration

Table 4 shows the parameter values for the CEQUEAU water temperature model after the calibration. These parameters were obtained for the period of 1990–2019. The obtained set of parameters is consistent in each case, with CRAYIN, CEVAPO and CORSOL having the most uniform values among all the parameters. The parameter TNAP is consistently chosen around 8.0°C, which is a good approximation of the actual groundwater temperature.

Calibration results (in terms of RMSE) are given in Figure 4. Overall, the different calibration strategies produce RMSE values ranging from 1.6 to 4.2°C. Best model performance was generally found in CPs centred on the Melezes' main stem (i.e., CP-1, CP-4, CP-6, CP-18, CP-82, CP-91, CP-118, CP-192, CP-296 and CP-326), which deliver RMSEs around 2.0°C in most of the cases. The lowest RMSE values were obtained using the parameters delivered with the CP-192, whereas the worst-performing main stem-located CPs are CP-84 and CP-91.

Conversely, the worst performance was generally observed at CPs located within headwater regions of the watershed. Indeed, the CP that performed worst across all calibration strategies is CP-141, which, from Figure 1, is seen to correspond to a headwater location comprising a fluvial lake (see Figure S2 in the Supplementary material). Poor behaviour at CPs corresponding to small streams and lakes is likely due to inadequacies in CEQUEAU's parameterisation. For example, in CPs corresponding to lakes or headwater streams (e.g., CP-35, CP-39, CP-141, CP-213, CP-270 and CP-350), CEQUEAU likely underestimates residence time and heat surface fluxes because it does not formally address lake stratification, surface flow velocities/residence times and/or additional surface heat inputs on large surfaces with no canopy.

Unlike the SSS-derived parameters, the MSS-derived parameters perform better across all individual CPs, even in those that showed poor performance using an SSS-derived parameter set. Here, the best RMSE value obtained across all CPs was 1.62°C (CP-435) using the multi_length strategy. The worst performing site (with the exception of CP-141) with an RMSE value of 3.09°C (for the weighted

TABLE 4 Water temperature parameters values obtained for each calibration strategy.

Id		COPROM	COLARG	CRAYSO	CRAYIN	CEVAPO	CCONVE	CRIGEL	TNAP	BASSOL	CORSOL
1	CP1	1.00	1.00	2.12	1.00	0.50	1.99	113.69	8.00	10.00	0.16
2	CP4	2.00	1.62	2.30	1.10	0.50	1.93	50.97	5.68	6.16	0.01
3	CP6	2.00	2.00	1.92	1.00	0.50	1.32	211.36	4.00	5.90	0.01
4	CP18	1.00	1.00	2.12	1.00	0.50	2.00	141.10	5.54	9.97	0.01
5	CP35	1.00	1.00	1.85	1.00	0.50	1.46	67.22	8.00	8.38	0.03
6	CP39	1.24	1.00	1.76	1.00	0.50	1.62	123.88	8.00	5.53	0.07
7	CP84	1.00	1.00	1.94	1.16	0.50	1.95	142.31	5.50	5.09	0.27
8	CP91	1.00	1.00	1.80	1.21	0.50	2.00	250.00	4.20	7.14	0.22
9	CP118	1.00	1.00	1.75	1.00	0.50	1.79	50.00	6.54	8.42	0.19
10	CP141	2.00	1.65	1.49	1.21	0.50	1.47	204.01	8.00	10.00	0.01
11	CP192	1.00	1.15	2.15	1.22	0.58	2.00	233.17	8.00	8.14	0.14
12	CP213	1.58	1.41	1.79	1.18	0.55	1.19	93.62	8.00	9.17	0.01
13	CP270	1.00	1.00	1.29	1.00	0.50	2.00	237.28	8.00	5.61	0.48
14	CP296	1.00	1.00	1.93	1.00	0.50	1.92	56.61	5.47	7.14	0.03
15	CP326	1.00	1.00	1.87	1.00	0.50	1.89	101.56	8.00	8.45	0.04
16	CP350	1.63	1.02	1.64	1.00	0.50	1.80	50.00	7.99	5.00	0.51
17	CP431	1.00	1.00	2.07	1.00	0.50	2.00	52.12	8.00	9.59	0.01
18	CP435	1.07	1.54	1.89	1.00	0.50	2.00	137.03	8.00	9.49	0.01
19	CP477	2.00	2.00	2.08	1.00	0.50	1.97	50.00	8.00	5.55	0.04
20	CP571	2.00	1.85	2.12	1.00	0.50	1.89	64.58	8.00	9.80	0.01
21	CP596	2.00	2.00	2.10	1.00	0.50	1.90	67.03	8.00	5.28	0.01
22	Arithmetic	1.36	1.30	1.90	1.05	0.51	1.81	118.93	7.09	7.61	0.11
23	Geometric	1.30	1.25	1.89	1.05	0.51	1.80	101.64	6.94	7.39	0.04
24	Harmonic	1.24	1.21	1.87	1.05	0.51	1.78	88.14	6.77	7.18	0.02
25	multi_area	2.00	1.39	2.22	1.52	0.50	1.63	74.36	7.81	9.14	0.05
26	multi_length	1.00	1.04	1.88	1.00	0.50	2.00	56.67	7.69	9.28	0.00
27	multi_pooled	1.83	1.00	2.21	1.32	0.50	1.82	51.55	7.91	6.36	0.00

Note: Rows 1–21 represent the single-site calibration strategy (SSS), 22–24 are the upscaling factors strategy (UFS), and the 25–27 rows are the parameter sets obtained with the multi-site strategy (MSS). The shade serves as separation between different sets of calibration strategies.

multi_area strategy) was CP-270 (located in an upstream tributary), comparing favourably to the SSS method, which yielded a worst RMSE of 3.62°C under all SSS runs. The same occurrence is repeated across CP-350, CP-431, CP-477, CP-571 and CP-596, highlighting how the MSS outperforms most of the SSS-delivered RMSEs.

The UFS-derived calibrations also outperform individual CP-based parameter sets. However, when compared with the MSS approach, it can be seen that despite their good performance, RMSEs are generally slightly poorer than those obtained using the MSS. Nevertheless, the differences in RMSE (between 0.01 and 0.1°C) are not significant when comparing the RMSEs obtained for the main river (i.e., CP-1, CP-4, CP-6, CP-84, CP-91, CP-118 and CP-192). Within all the three considered upscaling factors, the worst RMSE (again, excluding CP-141) was found with the Arithmetic mean (2.98°C at CP-270), and the best was 1.67°C in CP-435 using the Geometric and Harmonic means.

Figures 5 and 6 show the multi-annual means and scatter regression plots for both simulated and observed Landsat water temperature. Comparing simulated water temperatures with the MSS against the Landsat-derived water temperature suggests that both simulated and TIR-derived water temperatures range from around 0°C to 24°C throughout the basin. Note that data collected from the Landsat missions do not continuously span the whole calibration period, and only a subset of Landsat-derived temperature data were obtained for each individual CP. The time series length for Landsat data at each CP is presented in Table S2 of the Supplementary material. The absence of data at certain CPs/times is generally due to cloud cover obscuring the river channel at the moment of TIR image acquisition.

The simulated water temperatures fit well with the observed Landsat temperature, and for most cases, the CEQUEAU model reaches the annual mean observed values along the basin (see Figure 5).

Figure 6 allows us to see how well the simulated water temperature time series fits the derived Landsat temperature. Overall, the CEQUEAU model performs well in the temporal distribution of the

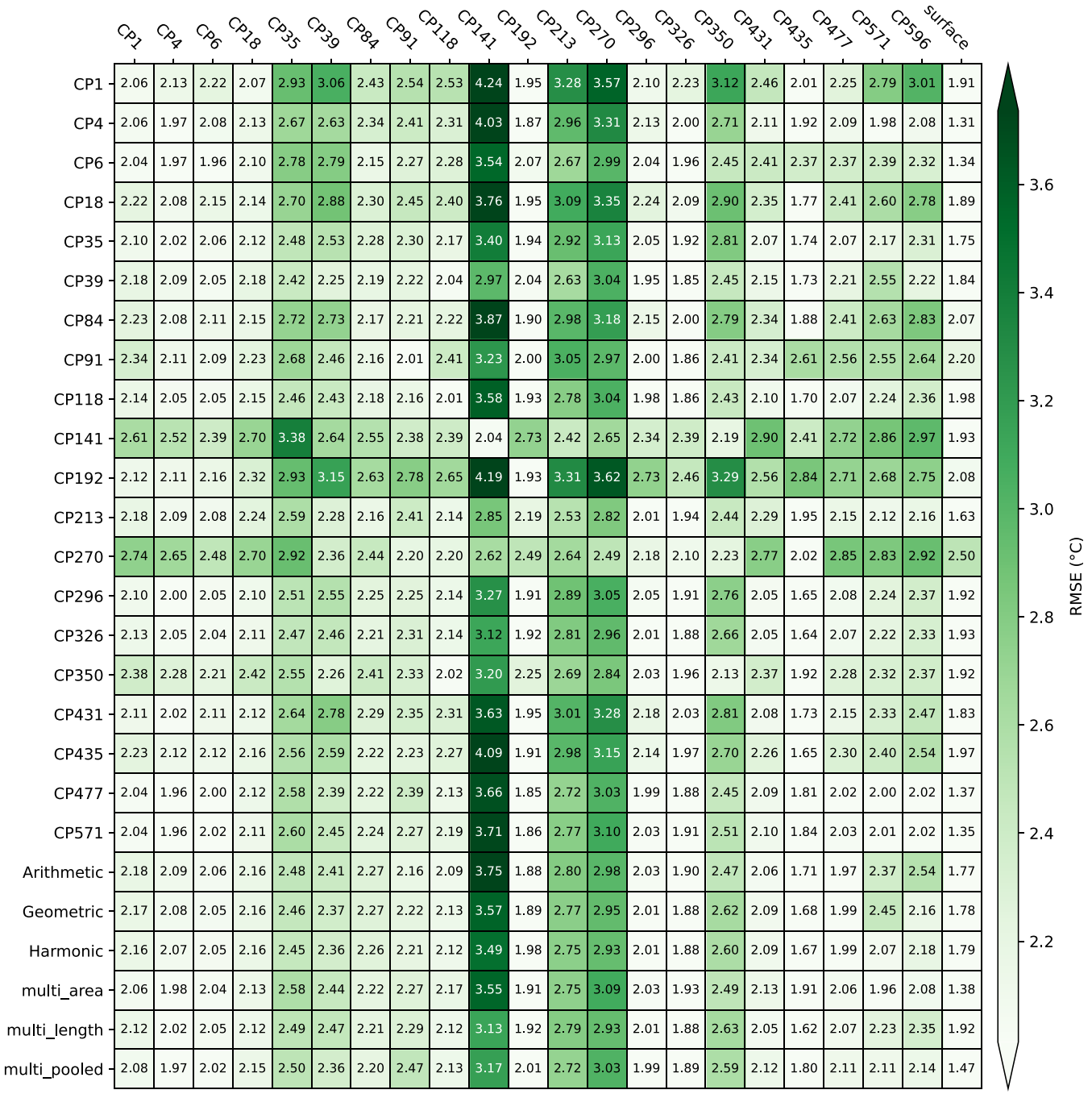

FIGURE 4 Heatmap comparing the obtained RMSEs for the different calibration strategies. The rows (*y*-axis) represent the CP point and/or the calibration strategy that was used to derive the parameter set, and the columns (*x*-axis) represent the result of evaluating these parameters at that specific location. The last column represents the surface station evaluation for validation purposes. RMSE is given in °C.

water temperature. There are some cases where the values were underestimated, such as in CP-596 and CP-477 ($R^2 = 0.81$ and $R^2 = 0.79$, respectively) and some others with a relatively large spread, as in CP-213 (R^2=0.72). In the downstream CPs such as CP-1, CP-4, CP-6 and CP-118, among the others, the agreement is very good, with $R^2 > 0.75$ in all the cases. However, this also shows that the CEQUEAU model does not reach the maximum Landsat-retrieved water temperature value (around 20°C) in those CPs.

3.3 | Comparison against surface station

The last column in Figure 4 shows the validation results achieved through simulating water temperature at the MFFP's surface water temperature station (see Section 2.7) with the various calibration strategies. In terms of the Single Site Strategy (SSS), CP-4, CP-6, CP-435 and CP-477 parameter sets perform better than the rest, reaching values of RMSE as low as 1.31°C in the CP-4. Validation performance

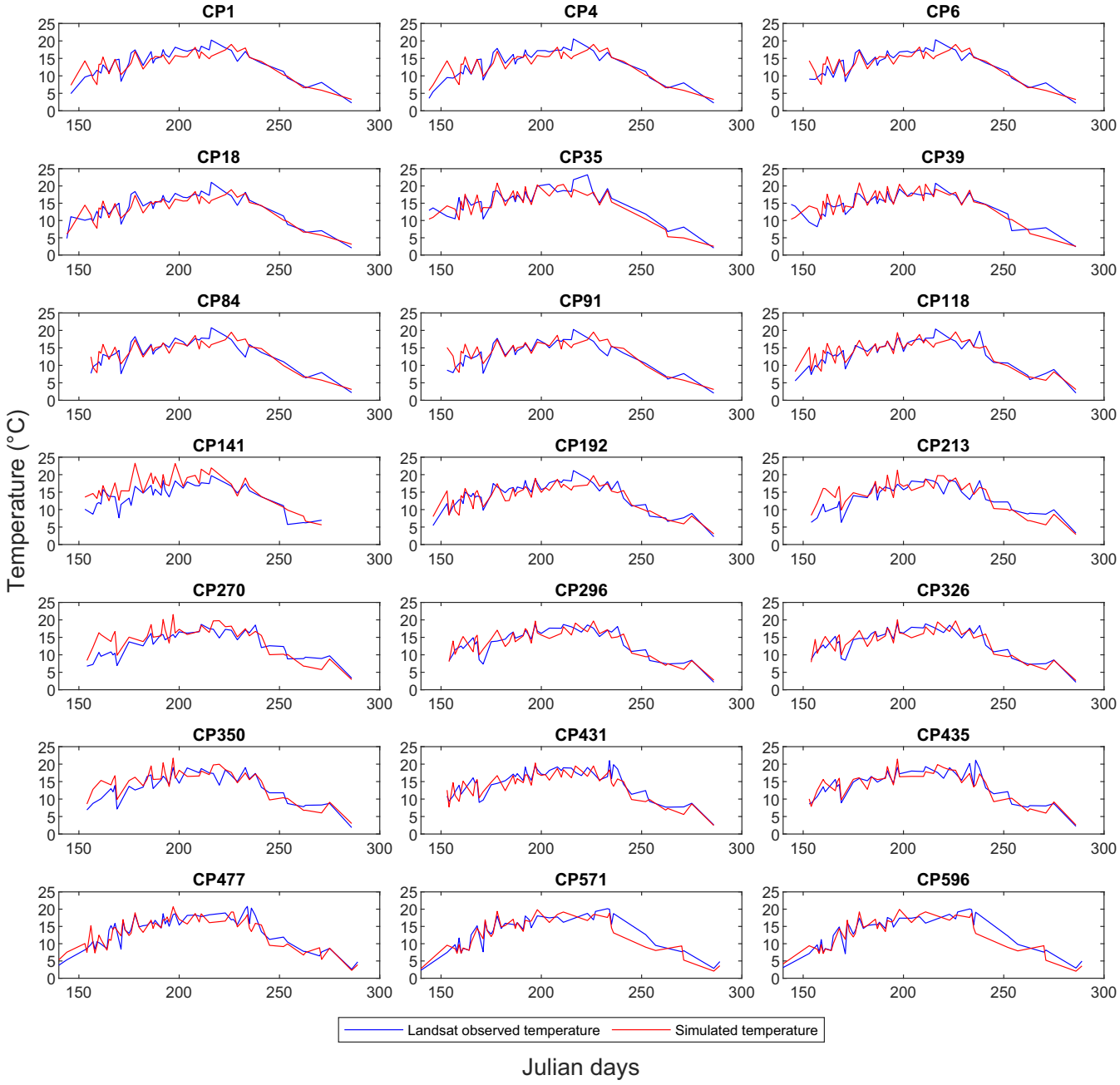

FIGURE 5 Multi-annual means simulated (red lines) and Landsat derived (blue lines) water temperature for each of the selected CPs. These multi-annual means were produced using the multi_area parameters set.

decreases when evaluating the surface station against headwater-derived parameters set as in CP-270, which delivered the highest RMSE (2.50°C).

The MSS-derived parameter sets increase the validation performance of the CEQUEAU model compared with the SSS. The best RMSE (1.38°C) was obtained with the multi_area method, whereas the worst RMSE of 1.92°C (using the multi_length strategy). This highlights the consistency of the MSS approach. Among the UFS, the Arithmetic mean delivered the best RMSE value (1.77°C), whereas the Harmonic performed worst (RMSE = 1.79°C). The best calculated RMSE with the MSS has significant differences with the best RMSE obtained with the UFS.

Based on these validation results, we selected the multi_area parameter set to explore how the model performs temporally using the surface station. The time series of observed and simulated water temperature are presented in Figure 7. In total, three summers of observed water temperatures are available. Figure 7A shows the multi-annual means of water temperatures for the period 2016 to 2019, and it is possible to see that the CEQUEAU model matches the onset of positive observed water temperature (blue line). This is a key

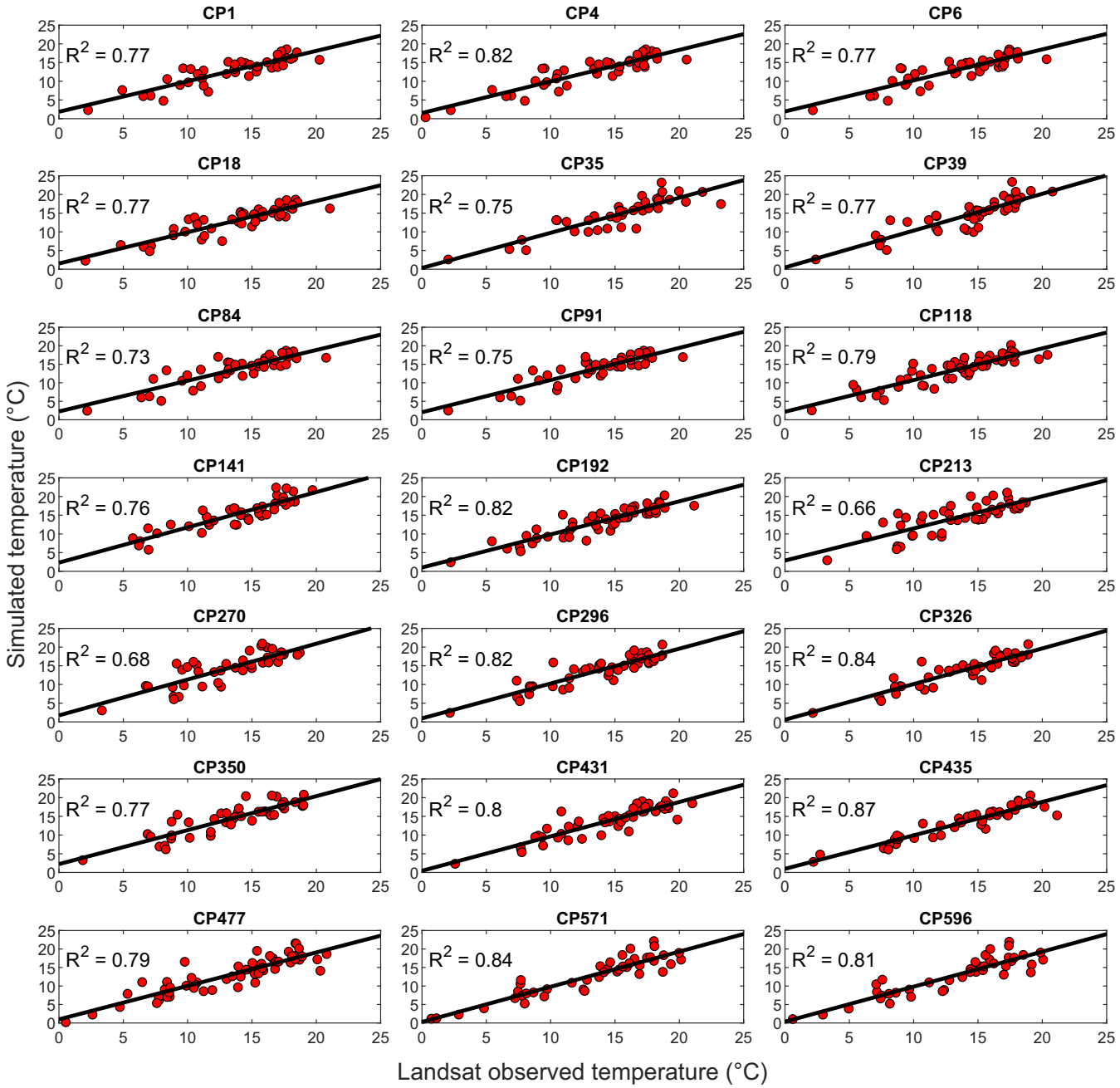

FIGURE 6 Scatter plots for observed (*x*-axis) Landsat-derived water temperature and simulations (*y*-axis) with the CEQUEAU model in each of the selected CPs. These diagrams were produced using the multi_area parameter set.

insight about the performance of the CEQUEAU model in Aux Mélèze river since this metric is likely to change across Canada under climate change conditions (see Daigle et al., 2010, for details). Although the model can represent such an important metric, its performance is reduced during the peak of the summer and the start of the autumn. This can be seen in Figure 7b, where a considerable portion of the points are below the regression line. Nonetheless, the $R^2 = 0.90$ coefficient confirms good agreement between the observed and simulated values. This positive result emphasizes the very strong ability of our calibration approach (MSS using TIR-derived temperature data) to provide parameter values that lead to accurate simulations of water temperature in Aux Mélèzes River.

The comparison between the surface observations, the simulated water temperature and the Landsat TIR-derived water temperature is shown in Figure 7c. The maximum surface observed (blue line) value for this time period is 17.71°C, while the maximum value obtained with the Landsat TIR images (blue dots) was 20.25°C. The overestimation of the observed water temperature was obtained during the summers of 2016 and 2017. In general, the comparison between the observed surface temperature and Landsat-derived temperature leads

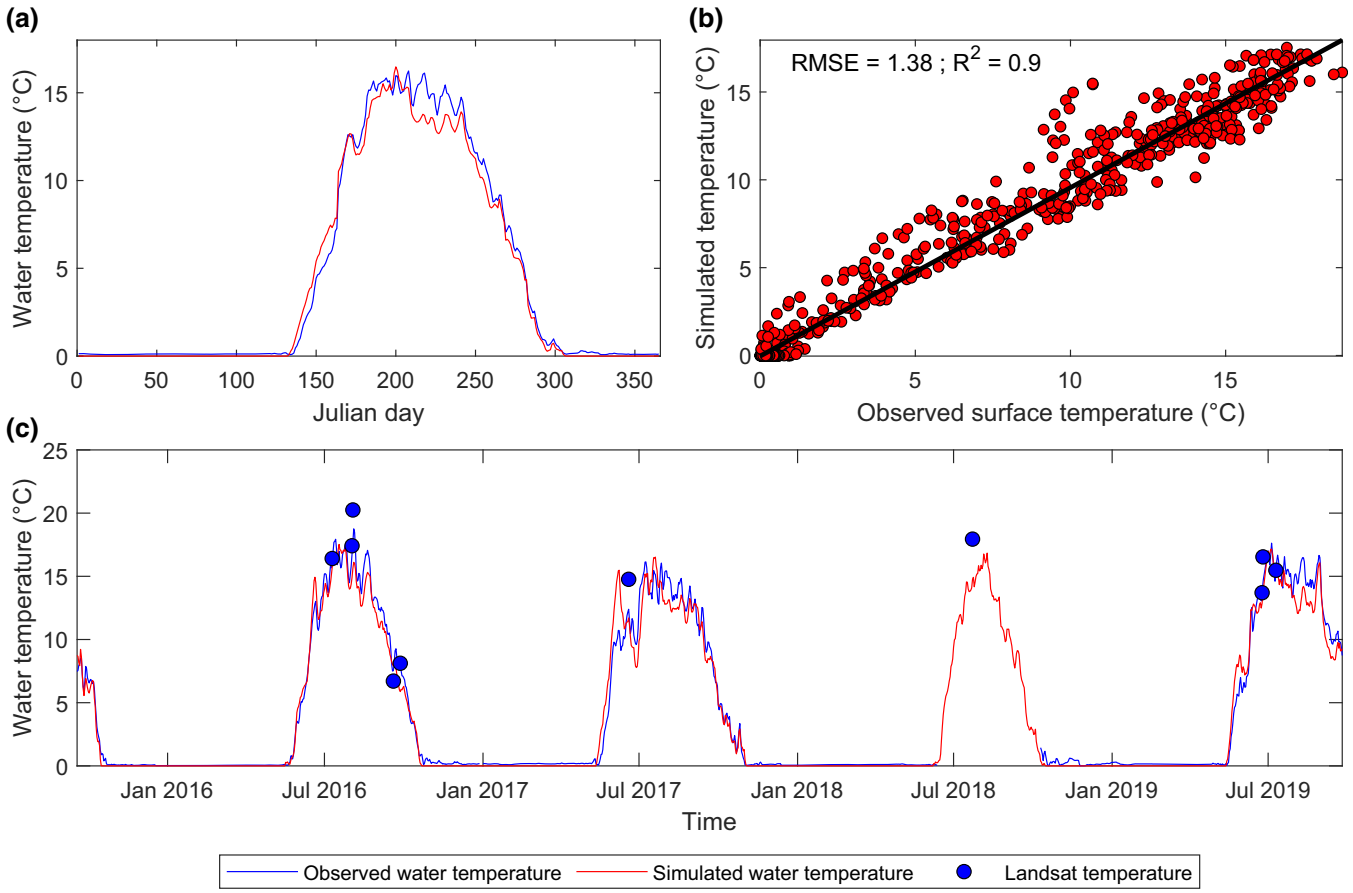

FIGURE 7 Validation of the simulated water temperature using the multi_area parameters set against the surface observations of water temperature and Landsat-derived temperature. (a) Represents the multi-annual means of observed (blue line) and simulated (red line) time series of water temperature for the period of 206–2019, (b) is the scatter plot of surface observed and simulated water temperature time series, and (c) shows the comparison between the surface observed water temperature (blue line), simulated water temperature (red line) and Landsat derived water temperature (blue dots) from 2016 to 2019.

to an RMSE = 1.40°C, which can be considered a very good estimation of the actual observed water temperature. The comparison of the simulated water temperature (red line) along with the Landsat-derived temperature for this time period delivered an RMSE = 2.03°C.

4 | DISCUSSION

The relative paucity of river discharge and water quality data in the Arctic and Subarctic makes river science very challenging in these regions. The development of new algorithms for processing space-borne and reanalysis data sources has given researchers new tools to exploit and develop new knowledge in these data-sparse regions. In this study, we combined information from ERA5 and Landsat TIR images with simulations from the CEQUEAU hydrological-water temperature model to produce consistent, accurate daily water temperature and flow time series in the Aux Mélèzes River, located in the northeastern Canadian Subarctic region. Although studies have been carried out describing water temperature and flow patterns in other regions of the Canadian Arctic (e.g., Stadnyk et al., 2020; Yang et al., 2014; Yang et al., 2021; Yang & Peterson, 2017), this represents the first effort to incorporate satellite-based thermal imagery along with hydrological/water temperature models over this region and is also the first to focus on the eastern portions of the Canadian Arctic.

4.1 | Water temperature estimation from satellite-based thermal imagery

The use of TIR-based instruments to monitor and quantify river temperature has gained attention during the last decades, particularly in remote areas where deploying in situ instruments that allow the measurement and monitoring of actual kinetic water temperature (Tk) is very challenging (Dugdale, 2016; Handcock et al., 2012). The radiant temperature measured by TIR-based instruments serves as a good approximation of the river temperature (Daigle et al., 2022; Dugdale, 2016; Handcock et al., 2012; Martí-Cardona et al., 2019; Tavares et al., 2020). However, given the high cost involved in 'conventional' monitoring campaigns across large rivers, such as the one involved in this study, would not be economically or logistically viable

(see Dugdale, 2016, for details). The use of space-borne Landsat TIR images allowed us to spatially understand the river temperature dynamic for a considerable time period over a remote area in the northeastern Canadian region.

Using the algorithm proposed by Martí-Cardona et al. (2019) to filter out mixed land-water pixels enabled us to estimate river temperature in reaches with widths ranging from 150 m in CP-431 to >350 m in CP-84. This greatly increases the applicability of satellite-derived river temperature data, meaning that they can now be used to constitute 'virtual' temperature gauging stations in relatively small watercourses. This overcomes the limitation highlighted in the recent study of Daigle et al. (2022), where only rivers with a minimum width ranging from 300 to 350 m were used to derive Landsat-based water temperature.

The comparison of the obtained Landsat-derived water temperature in CP-1 with the surface station has shown a high degree of accuracy (RMSE = 1.41°C) of the proposed method. This represents an improvement in the estimations given by Daigle et al. (2022), where an RMSE = 1.7°C was obtained in the same river. This indicated that filtering out the mixed bank river pixels improves the estimations of water temperature, as was stated by Martí-Cardona et al. (2019) in their study. Also, this result is in accordance with the estimations given by (Tavares et al., 2019), where after atmospherically correcting a set of TIR-based Landsat images and selecting (manually) only centred water pixels, they obtained an RMSE = 1.44°C. Our method allowed us to define automatically only pure water pixels distributed in space and time, avoiding human intervention, which reduces preprocessing time and errors by incorrectly choosing the wrong pixels.

4.2 | Surface flow simulations

The simulated discharge presented in Figure 2 suggests that ERA5 is a reliable source of information to obtain robust daily streamflow simulations. KGE = 0.86 and NSE = 0.79 give us confidence in our model's representation of the seasonal behaviour of the surface stream flow in the Aux Mélèze River. Unlike CEQUEAU's water temperature model component, the underlying hydrological model was calibrated using a single-site strategy. However, the validation results, when compared to observations from gauging station ID 103603 are equally good (KGE = 0.79, NSE = 0.65, RMSE = 80.75 m^3/s, and BIAS = −1.5 m^3/s). This validation highlights the strong ability of CEQUEAU to simulate high discharges at the outlet point while also correctly representing (reduced) flows in sub-basins. Although the obtained performance metrics are lower than at the principal calibration site (as expected), these results are still acceptable and reaffirm that the CEQUEAU model correctly represents the general seasonal patterns in the sub-basins within the Aux Mélèzes River. This, in turn, gives confidence in our reproduction of water temperature patterns throughout the basin. This study's results agree with similar investigations (e.g., Krogh et al., 2015), where ERA-Interim successfully allowed them to improve the streamflow simulation in a remote mountainous area in the Chilean Patagonia.

4.3 | Water temperature simulations

Among the calibration strategies considered in our study, the Single-Site-Strategy (SSS) produced the worst RMSE values when the derived parameters are evaluated in other CP locations. The Upscaling Factor Strategy (UFS) accounts for some spatial variability since it transfers local variability in the water temperature parameters to the basin scale. In our case, the Harmonic mean was found to be the most consistent in retrieving the lowest RMSE values throughout the different CP locations. This coincides with the results obtained by Khorsandi et al. (2022), where the harmonic mean was found to be the best upscaling factor to obtain global water temperature parameters for the CEQUEAU model. All the considered upscaling factors outperformed most of the SSS when comparing the performance in the individual CP locations.

However, comparing the obtained RMSE from UFS with those obtained with the Multi-Site Strategy (MSS), indicates that MSS can generate consistent improvements over UFS. MSS explicitly adjusts the parameters using all of the distributed Landsat-derived water temperature values in a single calibration. The latter ensures that the MSS approach represents the spatial variability better than the upscaling factors, as shown by the obtained RMSE values (Figure 4). Another fundamental advantage of the MSS is the computational time. The application of the UFS requires performing several single-site calibrations to compute the respective Upscaling Factor subsequently. In this particular case, the computation of each upscaling factor required 21 times the computational resources than the MSS. This, by itself, implies that MSS must be chosen over the UFS if future multi-site calibrations of the CEQUEAU model are required. This agrees with the result obtained by Khorsandi et al. (2022), where the reason for choosing MSS over UFS was mainly the computational time. Our study showed that even increasing the number of CP sites to derive basin scale parameters using Upscaling-Factors, the multi-site calibrations perform better. Indeed, in the case of the CEQUEAU model, the selected MSS that outperformed the rest was the multi_area, which coherently derived parameters taking the actual flow structure as a proxy to adjust the optimal parameters values. The simulated water temperature series for the different CPs considering the best performance calibration strategy (Figures 5 and 6) suggest that the CEQUEAU model simulations correctly fit into the range of variability of the estimated water temperature with Landsat TIR images. A biased behaviour is shown during summers and autumn for the period 2016 to 2019 when the simulations were compared against the surface-gauged station (see Figure 7a,c). The same pattern is shown in the whole considered calibration period, where the summer temperature is mostly underestimated during the end of the season (see Figure 5). As already mentioned in Section 4.1, the Landsat-derived radiance temperature is a good estimation of the surface water temperature. Therefore, our simulations produce coherent water temperature time series during the whole calibration period (1990–2019). The excellent degree of concordance between these water temperature observations and simulations from a model parameterized and calibrated purely using satellite/reanalysis data suggests that it is now

possible to generate long-term water temperature time series using information from satellite-based datasets and the CEQUEAU model.

4.4 | Limitations

This research presents some assumptions about how Aux Mélèze River hydrological and water temperature patterns work. Although hydrological calibration delivered excellent performance metrics, there are no observed data to confront the obtained subsurface and surface water fluxes. For example, the poor performance of spring peak flows is likely due to a misrepresentation of the physics of the snowmelt process, as stated by Landine et al. (1988). However, a large part of the uncertainty can be attributed to negative biases in ERA5 winter precipitation in the arctic zones (e.g., Tarek et al., 2020). This needs to be addressed in the future with better observation of snowmelt and precipitation near the study area.

Validating the TIR-derived water temperature with a longer time series of surface water temperature in such environments would be essential to define the existence of systematic biases between estimated TIR-based water temperature and surface water temperature. In our case, the difference between the obtained RMSE with the TIR-based water temperature and the RMSE comparing the simulated and surface water temperature is around 0.6°C. This would mean that evaluating the performance of the CEQUEAU model with TIR-based temperature would require some corrections for future applications since water temperature simulations taking ERA5 as reference data were already tested, and it showed good accuracy elsewhere in Canada (e.g., Gatien et al., 2022; Khorsandi et al., 2022).

5 | CONCLUSION

The main goal of this research was to demonstrate how simulated water temperature time series from a process-based water temperature model, parameterized using satellite and reanalysis data, can form a viable alternative to long-term in-situ time series of water temperature in remote Arctic regions, where problems relating to data-gathering and access persist. For those reasons, we framed this work in the context of the PUB problem, which has been widely explored in terms of flow simulations but lacks equivalent research focusing on water temperature in ungauged basins, particularly at sub-annual scales. This study constitutes the first application of the CEQUEAU model in a Subarctic environment. Our results show that the model is a very reliable tool to simulate both runoff and water temperature spatiotemporal patterns, even in the northeastern Canadian Arctic where conventional field data are almost absent. Indeed, our research shows the value of combining satellite-based remote sensing and meteorological reanalysis data for model parameterization and calibration. Our proposed approach suggests that the multi-site calibration strategy for calibrating the CEQUEAU model outperforms the single-site and upscaling factor calibration strategies for simulating water temperature throughout the entire basin, ultimately producing discharge and water temperature simulations equal or better to models calibrated and parameterized using 'conventional' data and approaches. This research emphasizes the strengths of the CEQUEAU model to simulate the main hydrological and river temperature patterns in complex environments such as the cold Canadian Subarctic region. Future research can now have confidence in using the CEQUEAU model to produce and assess future climate change studies, which will be fundamental for fisheries managers in the Arctic and Subarctic rivers.

FUNDING INFORMATION

This project was undertaken with the financial support of the Environment and Climate Change Canada.

DATA AVAILABILITY STATEMENT

The data that support the findings of this study are available in MIFI at https://www.cehq.gouv.qc.ca/hydrometrie/historique_donnees/default.asp. These data were derived from the following resources available in the public domain: — ERA5 reanalysis, https://cds.climate.copernicus.eu/#!/search?text=ERA5&type=dataset— TIR images, https://landsat.gsfc.nasa.gov/.

ORCID

Eisinhower Rincón https://orcid.org/0000-0003-4598-523X
André St-hilaire https://orcid.org/0000-0001-8443-5885
Normand E. Bergeron https://orcid.org/0000-0003-2413-6810
Stephen J. Dugdale https://orcid.org/0000-0003-3561-4216

REFERENCES

Arsenault, R., Poulin, A., Côté, P., & Brissette, F. (2014). Comparison of stochastic optimization algorithms in hydrological model calibration. *Journal of Hydrologic Engineering*, *19*, 1374–1384. https://doi.org/10.1061/(ASCE)HE.1943-5584.0000938

Bolduc, C., & Lamoureux, S. F. (2018). Multiyear variations in high Arctic river temperatures in response to climate variability. *Arctic Science*, *4*, 605–623. https://doi.org/10.1139/as-2017-0053

Caissie, D. (2006). The thermal regime of rivers: A review. *Freshwater Biology*, *51*, 1389–1406. https://doi.org/10.1111/j.1365-2427.2006.01597.x

Charron, C., St-Hilaire, A., Ouarda, T. B., & van den Heuvel, M. R. (2021). Water temperature and hydrological modelling in the context of environmental flows and future climate change: Case study of the Wilmot River (Canada). *Water*, *13*, 2101. https://doi.org/10.3390/w13152101

Cherkauer, K. A., Burges, S. J., Handcock, R. N., Kay, J. E., Kampf, S. K., & Gillespie, A. R. (2005). Assessing satellite-based and aircraft-based thermal infrared remote sensing for monitoring pacific northwest river temperature. *Journal of the American Water Resources Association*, *41*, 1149–1159. https://doi.org/10.1111/j.1752-1688.2005.tb03790.x

Daigle, A., Boyer, C., & Légaré, A. (2022). Modeling of the thermal regime of rivers subject to seasonal ice cover using data from different sources and temporal resolutions. *Canadian Water Resources Journal/Revue canadienne des ressources hydriques*, *48*, 1–17. https://doi.org/10.1080/07011784.2022.2140604

Daigle, A., Ouarda, T. B., & Bilodeau, L. (2010). Comparison of parametric and non-parametric estimations of the annual date of positive water temperature onset. *Journal of Hydrology*, *390*, 75–84. https://doi.org/10.1016/j.jhydrol.2010.06.032

DeBeer, C. M., Wheater, H. S., Carey, S. K., & Chun, K. P. (2016). Recent climatic, cryospheric, and hydrological changes over the interior of western Canada: A review and synthesis. *Hydrology and Earth System Sciences*, *20*, 1573–1598. https://doi.org/10.5194/hess-20-1573-2016

Déry, S. J., Stadnyk, T. A., MacDonald, M. K., & Gauli-Sharma, B. (2016). Recent trends and variability in river discharge across northern Canada. *Hydrology and Earth System Sciences*, *20*, 4801–4818. https://doi.org/10.5194/hess-20-4801-2016

Ding, Q., Wallace, J. M., Battisti, D. S., Steig, E. J., Gallant, A. J. E., Kim, H.-J., & Geng, L. (2014). Tropical forcing of the recent rapid Arctic warming in northeastern Canada and Greenland. *Nature*, *509*, 209–212. https://doi.org/10.1038/nature13260

Dugdale, S. J. (2016). A practitioner's guide to thermal infrared remote sensing of rivers and streams: Recent advances, precautions and considerations. *WIREs Water*, *3*, 251–268. https://doi.org/10.1002/wat2.1135_eprint

Dugdale, S. J., Allen Curry, R., St-Hilaire, A., & Andrews, S. N. (2018). Impact of future climate change on water temperature and thermal habitat for keystone fishes in the lower Saint John River, Canada. *Water Resources Management*, *32*, 4853–4878. https://doi.org/10.1007/s11269-018-2057-7

Dugdale, S. J., St-Hilaire, A., & Allen Curry, R. (2017). Automating drainage direction and physiographic inputs to the CEQUEAU hydrological model: Sensitivity testing on the lower Saint John River watershed, Canada. *Journal of Hydroinformatics*, *19*, 469–492. https://doi.org/10.2166/hydro.2017.051

Duguay-Tetzlaff, A., Bento, V., Göttsche, F., Stöckli, R., Martins, J., Trigo, I., Olesen, F., Bojanowski, J., da Camara, C., & Kunz, H. (2015). Meteosat land surface temperature climate data record: Achievable accuracy and potential uncertainties. *Remote Sensing*, *7*, 13139–13156. https://doi.org/10.3390/rs71013139

Duguay-Tetzlaff, A., Bento, V. A., & Stöckli, R. (2017). *Algorithm theoretical basis document for land surface temperature (LST)*. Technical Report 1 CM-SAF. https://doi.org/10.5676/EUM_SAF_CM/LST_METEOSAT/V001

Ermida, S. L., Soares, P., Mantas, V., Göttsche, F.-M., & Trigo, I. F. (2020). Google earth engine open-source code for land surface temperature estimation from the landsat series. *Remote Sensing*, *12*, 1471. https://doi.org/10.3390/rs12091471

Essou, G. R., Sabarly, F., Lucas-Picher, P., Brissette, F., & Poulin, A. (2016). Can precipitation and temperature from meteorological reanalyses be used for hydrological modeling? *Journal of Hydrometeorology*, *17*, 1929–1950. https://doi.org/10.1175/JHM-D-15-0138.1

Ficklin, D. L., Stewart, I. T., & Maurer, E. P. (2013). Effects of climate change on stream temperature, dissolved oxygen, and sediment concentration in the Sierra Nevada in California. *Water Resources Research*, *49*, 2765–2782. https://doi.org/10.1002/wrcr.20248

Foster, J. L., Robinson, D. A., Hall, D. K., & Estilow, T. W. (2008). Spring snow melt timing and changes over Arctic lands. *Polar Geography*, *31*, 145–157. https://doi.org/10.1080/10889370802580185

Gatien, P., Arsenault, R., Martel, J.-L., & St-Hilaire, A. (2022). Using the ERA5 and ERA5-Land reanalysis datasets for river water temperature modelling in a data-scarce region. *Canadian Water Resources Journal/Revue canadienne des ressources hydriques*, *0*, 1–18. https://doi.org/10.1080/07011784.2022.2113917

Gupta, H. V., Kling, H., Yilmaz, K. K., & Martinez, G. F. (2009). Decomposition of the mean squared error and NSE performance criteria: Implications for improving hydrological modelling. *Journal of Hydrology*, *377*, 80–91. https://doi.org/10.1016/j.jhydrol.2009.08.003

Handcock, R., Gillespie, A., Cherkauer, K., Kay, J., Burges, S., & Kampf, S. (2006). Accuracy and uncertainty of thermal-infrared remote sensing of stream temperatures at multiple spatial scales. *Remote Sensing of Environment*, *100*, 427–440. https://doi.org/10.1016/j.rse.2005.07.007

Handcock, R. N., Torgersen, C. E., Cherkauer, K. A., Gillespie, A. R., Tockner, K., Faux, R. N., & Tan, J. (2012). Thermal infrared remote sensing of water temperature in riverine landscapes. In *Fluvial Remote Sensing for Science and Management* (pp. 85–113). John Wiley & Sons, Ltd. https://doi.org/10.1002/9781119940791.ch5

Hannah, D. M., & Garner, G. (2015). River water temperature in the United Kingdom: Changes over the 20th century and possible changes over the 21st century. *Progress in Physical Geography*, *39*, 68–92. https://doi.org/10.1177/0309133314550669

Hansen, N., & Ostermeier, A. (2001). Completely derandomized self-adaptation in evolution strategies. *Evolutionary Computation*, *9*, 159–195. https://doi.org/10.1162/106365601750190398

Hette-Tronquart, N., Roussel, J. M., Dumont, B., Archaimbault, V., Pont, D., Oberdorff, T., & Belliard, J. (2013). Variability of water temperature may influence food-chain length in temperate streams. *Hydrobiologia*, *718*, 159–172. https://doi.org/10.1007/s10750-013-1613-7

Hill, R. A., Hawkins, C. P., & Jin, J. (2014). Predicting thermal vulnerability of stream and river ecosystems to climate change. *Climatic Change*, *125*, 399–412. https://doi.org/10.1007/s10584-014-1174-4

Hinzman, L. D., Bettez, N. D., Bolton, W. R., Chapin, F. S., Dyurgerov, M. B., Fastie, C. L., Griffith, B., Hollister, R. D., Hope, A., Huntington, H. P., Jensen, A. M., Jia, G. J., Jorgenson, T., Kane, D. L., Klein, D. R., Kofinas, G., Lynch, A. H., Lloyd, A. H., McGuire, A. D., … Yoshikawa, K. (2005). Evidence and implications of recent climate change in Northern Alaska and other Arctic regions. *Climatic Change*, *72*, 251–298. https://doi.org/10.1007/s10584-005-5352-2

Hori, M. (2021). Near-daily monitoring of surface temperature and channel width of the six largest Arctic rivers from space using GCOM-C/SGLI. *Remote Sensing of Environment*, *263*, 112538. https://doi.org/10.1016/j.rse.2021.112538

Hrachowitz, M., Savenije, H. H., Blöschl, G., McDonnell, J. J., Sivapalan, M., Pomeroy, J. W., Arheimer, B., Blume, T., Clark, M. P., Ehret, U., Fenicia, F., Freer, J. E., Gelfan, A., Gupta, H. V., Hughes, D. A., Hut, R. W., Montanari, A., Pande, S., Tetzlaff, D., … Cudennec, C. (2013). A decade of predictions in ungauged basins (PUB)-A review. *Hydrological Sciences Journal*, *58*, 1198–1255. https://doi.org/10.1080/02626667.2013.803183

Isaak, D. J., & Rieman, B. E. (2013). Stream isotherm shifts from climate change and implications for distributions of ectothermic organisms. *Global Change Biology*, *19*, 742–751. https://doi.org/10.1111/gcb.12073

Jiang, Q., Li, W., Fan, Z., He, X., Sun, W., Chen, S., Wen, J., Gao, J., & Wang, J. (2021). Evaluation of the ERA5 reanalysis precipitation dataset over Chinese Mainland. *Journal of Hydrology*, *595*, 125660. https://doi.org/10.1016/j.jhydrol.2020.125660

Khorsandi, M., St-Hilaire, A., & Arsenault, R. (2022). Multisite calibration of a semi-distributed hydrologic and thermal model in a large canadian watershed. *Hydrological Sciences Journal*, *67*, 2147–2174. https://doi.org/10.1080/02626667.2022.2132161

Klemetsen, A., Amundsen, P.-A., Dempson, J. B., Jonsson, B., Jonsson, N., O'Connell, M. F., & Mortensen, E. (2003). Atlantic salmon *Salmo salar* L., brown trout *Salmo trutta* L. and Arctic charr *Salvelinus alpinus* (L.): A review of aspects of their life histories. *Ecology of Freshwater Fish*, *12*, 1–59. https://doi.org/10.1034/j.1600-0633.2003.00010.x

Krogh, S. A., Pomeroy, J. W., & McPhee, J. (2015). Physically based mountain hydrological modeling using reanalysis data in Patagonia. *Journal of Hydrometeorology*, *16*, 172–193. https://doi.org/10.1175/JHM-D-13-0178.1

Kwak, J., St-Hilaire, A., & Chebana, F. (2016). A comparative study for water temperature modelling in a small basin, the Fourchue River, Quebec, Canada. *Hydrological Sciences Journal*, *62*, 1–12. https://doi.org/10.1080/02626667.2016.1174334

Kwak, J., St-Hilaire, A., Chebana, F., & Kim, G. (2017). Summer season water temperature modeling under the climate change: Case study for

Fourchue River, Quebec, Canada. *Water*, *9*, 346. https://doi.org/10.3390/w9050346

Lammers, R. B., Shiklomanov, A. I., Vörösmarty, C. J., Fekete, B. M., & Peterson, B. J. (2001). Assessment of contemporary Arctic river runoff based on observational discharge records. *Journal of Geophysical Research: Atmospheres*, *106*, 3321–3334. https://doi.org/10.1029/2000JD900444

Landine, P. G., Granger, R. J., & Gray, D. M. (1988). Evaluation of snowmelt models for application in permafrost environments. Technical Report Environment Canada Contract KW504-7-1554 Saskatoon, Saskatchewan.

Larsen, J., Anisimov, O., Constable, A., Hollowed, A., Maynard, N., Prestrud, P., Prowse, T., & Stone, J. (2014). Chapter 28: Polar regions. In V. R. Barros, C. B. Field, D. J. Dokken, M. D. Mastrandrea, K. J. Mach, T. E. Bilir, M. Chatterjee, K. L. Ebi, Y. O. Estrada, R. C. Genova, B. Girma, E. S. Kissel, A. N. Levy, S. MacCracken, P. R. Mastrandrea, & L. L. White (Eds.), *Climate Change 2014: Impacts, adaptation, and vulnerability. Part B: Regional aspects. Contribution of Working Group II to the Fifth Assessment Report of the Intergovernmental Panel on Climate Change* (pp. 1567–1612). Cambridge University Press.

Martí-Cardona, B., Prats, J., & Niclòs, R. (2019). Enhancing the retrieval of stream surface temperature from Landsat data. *Remote Sensing of Environment*, *224*, 182–191. https://doi.org/10.1016/j.rse.2019.02.007

Morales-Marín, L., Sanyal, P., Kadowaki, H., Li, Z., Rokaya, P., & Lindenschmidt, K. (2019). A hydrological and water temperature modelling framework to simulate the timing of river freeze-up and ice-cover breakup in large-scale catchments. *Environmental Modelling & Software*, *114*, 49–63. https://doi.org/10.1016/j.envsoft.2019.01.009

Morin, G., & Paquet, P. (2007). *Modèle hydrologique CEQUEAU*. INRS-ETE.

Nash, J., & Sutcliffe, J. (1970). River flow forecasting through conceptual models part I—A discussion of principles. *Journal of Hydrology*, *10*, 282–290. https://doi.org/10.1016/0022-1694(70)90255-6

Odusanya, A., Mehdi, B., Schürz, C., Oke, A., Awokola, O., Awomeso, J., Adejuwon, J., & Schulz, K. (2018). Multi-site calibration and validation of SWAT with satellite-based evapotranspiration in a data sparse catchment in southwestern Nigeria. *Hydrology and Earth System Sciences Discussions*, *23*, 1–37. https://doi.org/10.5194/hess-2018-170

Ouellet-Proulx, S., St-Hilaire, A., & Boucher, M. A. (2019). Implication of evaporative loss estimation methods in discharge and water temperature modelling in cool temperate climates. *Hydrological Processes*, *33*, 2867–2884. https://doi.org/10.1002/hyp.13534

Parlee, B., & Furgal, C. (2012). Well-being and environmental change in the arctic: A synthesis of selected research from Canada's international polar year program. *Climatic Change*, *115*, 13–34. https://doi.org/10.1007/S10584-012-0588-0/FIGURES/6

Poesch, M. S., Chavarie, L., Chu, C., Pandit, S. N., & Tonn, W. (2016). Climate change impacts on freshwater fishes: A canadian perspective. *Fisheries*, *41*, 385–391. https://doi.org/10.1080/03632415.2016.1180285

Power, G. (1976). History of the hudson's bay company salmon fisheries in the ungava bay region. *Polar Record*, *18*, 151–161. https://doi.org/10.1017/S0032247400000061

Reist, J. D., Wrona, F. J., Prowse, T. D., Power, M., Dempson, J. B., Beamish, R. J., King, J. R., Carmichael, T. J., & Sawatzky, C. D. (2006). General effects of climate change on arctic fishes and fish populations. *Ambio*, *35*, 370–380. https://doi.org/10.1579/0044-7447(2006)35[381:AOOEOC]2.0.CO;2

Reist, J. D., Wrona, F. J., Prowse, T. D., Power, M., Dempson, J. B., King, J. R., & Beamish, R. J. (2006). An overview of effects of climate change on selected Arctic freshwater and anadromous fishes. *Ambio*, *35*, 381–387. https://doi.org/10.1579/0044-7447(2006)35[381:AOOEOC]2.0.CO;2

Samaniego, L., Kumar, R., & Attinger, S. (2010). Multiscale parameter regionalization of a grid-based hydrologic model at the mesoscale. *Water Resources Research*, *46*, W05523. https://doi.org/10.1029/2008WR007327

Shen, H., Tolson, B. A., & Mai, J. (2022). Time to update the split-sample approach in hydrological model calibration. *Water Resources Research*, *58*, e2021WR031523. https://doi.org/10.1029/2021WR031523

Sivapalan, M., Takeuchi, K., Franks, S. W., Gupta, V. K., Karambiri, H., Lakshmi, V., Liang, X., McDonnell, J. J., Mendiondo, E. M., O'Connell, P. E., Oki, T., Pomeroy, J. W., Schertzer, D., Uhlenbrook, S., & Zehe, E. (2003). IAHS decade on predictions in ungauged Basins (PUB), 2003–2012: Shaping an exciting future for the hydrological sciences. *Hydrological Sciences Journal*, *48*, 857–880. https://doi.org/10.1623/hysj.48.6.857.51421

St Hilaire, A., Boucher, M.-A., Chebana, F., Ouellet-Proulx, S., Zhou, Q. X., Larabi, S., Dugdale, S., & Latraverse, M. (2015). Breathing new life to an older model: The CEQUEAU tool for flow and water temperature simulations and forecasting. In *22nd Canadian Hydrotechnical Conference*. (p. 10). Montreal, Quebec, Canada: Canadian Society for Civil Engineering.

St. Jacques, J.-M., & Sauchyn, D. J. (2009). Increasing winter baseflow and mean annual streamflow from possible permafrost thawing in the Northwest Territories, Canada. *Geophysical Research Letters*, *36*, L01401. https://doi.org/10.1029/2008GL035822

Stadnyk, T. A., MacDonald, M. K., Tefs, A., Déry, S. J., Koenig, K., Gustafsson, D., Isberg, K., & Arheimer, B. (2020). Hydrological modeling of freshwater discharge into hudson bay using hype. *Elementa: Science of the Anthropocene*, *8*, 43. https://doi.org/10.1525/elementa.439

St-Hilaire, A., Morin, G., El-Jabi, N., & Caissie, D. (2000). Water temperature modelling in a small forested stream: Implication of forest canopy and soil temperature. *Canadian Journal of Civil Engineering*, *27*, 1095–1108. https://doi.org/10.1139/cjce-27-6-1095

Svenning, M.-A., Sandem, K., Halvorsen, M., Kanstad-Hanssen, Ø., Falkegård, M., & Borgstrøm, R. (2016). Change in relative abundance of Atlantic salmon and Arctic charr in Veidnes River, Northern Norway: a possible effect of climate change? *Hydrobiologia*, *783*, 145–158. https://doi.org/10.1007/s10750-016-2690-1

Tarek, M., Brissette, F. P., & Arsenault, R. (2020). Evaluation of the ERA5 reanalysis as a potential reference dataset for hydrological modelling over North America. *Hydrology and Earth System Sciences*, *24*, 2527–2544. https://doi.org/10.5194/hess-24-2527-2020

Tavares, M. H., Cunha, A. H. F., Motta-Marques, D., Ruhoff, A. L., Cavalcanti, J. R., Fragoso, C. R., Bravo, J. M., Munar, A. M., Fan, F. M., & Rodrigues, L. H. R. (2019). Comparison of methods to estimate lake-surface-water temperature using landsat 7 ETM+ and MODIS imagery: Case study of a large shallow subtropical lake in Southern Brazil. *Water (Switzerland)*, *11*, 1–21. https://doi.org/10.3390/w11010168

Tavares, M. H., Cunha, A. H. F., Motta-Marques, D., Ruhoff, A. L., Fragoso, C. R., Munar, A. M., & Bonnet, M.-P. (2020). Derivation of consistent, continuous daily river temperature data series by combining remote sensing and water temperature models. *Remote Sensing of Environment*, *241*, 111721. https://doi.org/10.1016/j.rse.2020.111721

van Vliet, M. T., Franssen, W. H., Yearsley, J. R., Ludwig, F., Haddeland, I., Lettenmaier, D. P., & Kabat, P. (2013). Global river discharge and water temperature under climate change. *Global Environmental Change*, *23*, 450–464. https://doi.org/10.1016/j.gloenvcha.2012.11.002

Vaughan, D., Comiso, J., Allison, I., Carrasco, J., Kaser, G., Kwok, R., Mote, P., Murray, T., Paul, F., & Ren, J. (2013). Observations: cryosphere. In T. F. Stocker, D. Qin, G.-K. Plattner, M. Tignor, S. K. Allen, J. Boschung, A. Nauels, & Y. Xi (Eds.), *Climate change 2013: The physical science basis. Contribution of Working Group I to the Fifth Assessment Report of the Intergovernmental Panel on Climate Change* (pp. 317–382). Cambridge University Press. https://doi.org/10.1007/978-1-4020-4411-3_53

Webb, B. W., Hannah, D. M., Moore, R. D., Brown, L. E., & Nobilis, F. (2008). Recent advances in stream and river temperature research. *Hydrological Processes*, *22*, 902–918. https://doi.org/10.1002/hyp.6994

Yang, D., Marsh, P., & Ge, S. (2014). Heat flux calculations for Mackenzie and Yukon Rivers. *Polar Science*, *8*, 232–241. https://doi.org/10.1016/j.polar.2014.05.001

Yang, D., & Peterson, A. (2017). River water temperature in relation to local air temperature in the Mackenzie and Yukon Basins. *Arctic*, *70*, 47–58. https://doi.org/10.14430/arctic4627

Yang, D., Shrestha, R. R., Lung, J. L. Y., Tank, S., & Park, H. (2021). Heat flux, water temperature and discharge from 15 northern Canadian rivers draining to Arctic Ocean and Hudson Bay. *Global and Planetary Change*, *204*, 103577. https://doi.org/10.1016/j.gloplacha.2021.103577

SUPPORTING INFORMATION

Additional supporting information can be found online in the Supporting Information section at the end of this article.

How to cite this article: Rincón, E., St-hilaire, A., Bergeron, N. E., & Dugdale, S. J. (2023). Combining Landsat TIR-imagery data and ERA5 reanalysis information with different calibration strategies to improve simulations of streamflow and river temperature in the Canadian Subarctic. *Hydrological Processes*, *37*(10), e15008. https://doi.org/10.1002/hyp.15008